

DISCOVERY OF THE ECLIPSING DETACHED DOUBLE WHITE DWARF BINARY NLTT 11748

JUSTIN D. R. STEINFADT¹, DAVID L. KAPLAN^{2,3}, AVI SHPORER^{1,4}, LARS BILDSTEN^{1,2}, AND STEVE B. HOWELL⁵

Accepted for publication in ApJ Letters, 2010 May 11

ABSTRACT

We report the discovery of the first eclipsing detached double white dwarf (WD) binary. In a pulsation search, the low-mass helium core WD NLTT 11748 was targeted for fast (≈ 1 minute) differential photometry with the Las Cumbres Observatory’s Faulkes Telescope North. Rather than pulsations, we discovered ≈ 180 s 3%–6% dips in the photometry. Subsequent radial velocity measurements of the primary white dwarf from the Keck telescope found variations with a semi-amplitude $K_1 = 271 \pm 3$ km s⁻¹, and confirmed the dips as eclipses caused by an orbiting WD with a mass $M_2 = 0.648\text{--}0.771 M_\odot$ for $M_1 = 0.1\text{--}0.2 M_\odot$. We detect both the primary and secondary eclipses during the $P_{\text{orb}} = 5.64$ hr orbit and measure the secondary’s brightness to be $3.5\% \pm 0.3\%$ of the primary at SDSS- g' . Assuming that the secondary follows the mass–radius relation of a cold C/O WD and including the effects of microlensing in the binary, the primary eclipse yields a primary radius of $R_1 = 0.043\text{--}0.039 R_\odot$ for $M_1 = 0.1\text{--}0.2 M_\odot$, consistent with the theoretically expected values for a helium core WD with a thick, stably burning hydrogen envelope. Though nearby (at ≈ 150 pc), the gravitational wave strain from NLTT 11748 is likely not adequate for direct detection by the *Laser Interferometer Space Antenna*. Future observational efforts will determine M_1 , yielding accurate WD mass–radius measurement of both components, as well as a clearer indication of the binary’s fate once contact is reached.

Subject headings: binaries: eclipsing—stars: individual (NLTT 11748)—white dwarfs

1. INTRODUCTION

Double white dwarfs (WDs) in tight enough ($P_{\text{orb}} < \text{day}$) binaries to reach contact in a Hubble time are expected on theoretical grounds (Nelemans et al. 2001), and are presumed to be the progenitors of highly variable objects: R CrB stars, AM CVn binaries, and Type Ia supernovae (Iben & Tutukov 1984; Webbink 1984). However, examples of these systems are rare, with only 10 known prior to our work (Nelemans et al. 2001; Badenes et al. 2009; Mullally et al. 2009; Kilic et al. 2009; Marsh et al. 2010; Kulkarni & van Kerkwijk 2010). Many of these binaries are of immediate interest for the *Laser Interferometer Space Antenna* (LISA), providing ‘verification’ sources loud enough to be detected in space (Nelemans 2009).

Spectral measurements of the high proper motion object NLTT 11748 by Kawka & Vennes (2009) revealed it to be a low-mass ($< 0.2 M_\odot$) helium core WD with $\log g = 6.2 \pm 0.15$ and $T_{\text{eff}} = 8540 \pm 50$ K and an H-rich (DA) atmosphere. The strong expectation that low-mass He WDs can only be formed in common envelope events led Kawka & Vennes (2009) to note that this object was likely a binary. Indeed, they found a 40 km s^{-1} velocity difference between two measured spectra. NLTT 11748 was originally targeted in a ZZ Ceti like pulsation search based on theoretical calculations and the $\log g$ and T_{eff} measurements (Steinfadt et al. 2010). In this failed pulsation search, our rapid (≈ 1 minute) differential photometry with the Las Cumbres Observatory’s Faulkes Telescope North (FTN) revealed ≈ 180 s 3%–6% dips, which were confirmed

by Keck spectroscopy to be primary and secondary eclipses from a $\approx 0.7 M_\odot$ faint C/O WD companion orbiting at 5.6 hr.

NLTT 11748 joins the growing class (Kawka et al. 2006; Kilic et al. 2007; Mullally et al. 2009; Kilic et al. 2009; Marsh et al. 2010; Kulkarni & van Kerkwijk 2010; Badenes et al. 2009) of WD binaries where the low-mass WD is a very low-mass ($< 0.2 M_\odot$) helium core WD. These are made when the lower mass star overfills its Roche lobe at the base of the red giant branch (van Kerkwijk et al. 1996; Callanan et al. 1998; Bassa et al. 2006a), triggering a common envelope event that leads to an in-spiral of the now exposed low-mass He core to a shorter orbital period. Theoretical work has found a dichotomy in the evolution of these low-mass He core WDs (Driebe et al. 1999; Serenelli et al. 2002; Panei et al. 2007) that dramatically impact their cooling rate. For masses $\gtrsim 0.2 M_\odot$ (metallicity dependent), the H envelope undergoes shell flashes that reduce its mass, eventually allowing the WD to cool rapidly. However, less massive ($< 0.2 M_\odot$) WDs undergo stable H burning for gigayears, dramatically slowing their evolution and keeping them brighter for much longer than expected.

Our observations are summarized in Section 2, demonstrating that the companion to NLTT 11748 is a cold ($T_{\text{eff}} \lesssim 7400$ K), old (1.5–3 Gyr) C/O WD. We show in Section 3 that eclipse modeling yields the first radius measurement of an extremely low-mass WD. We close in Section 4 by discussing the value of additional measurements for constraining WD mass–radius relations.

2. OBSERVATIONS

We targeted NLTT 11748 as part of an observational search for ZZ Ceti like pulsations from low-mass He core WDs (Steinfadt et al. 2008b, 2010). Our photometric discovery led to our Keck spectroscopy, both described here.

2.1. *Faulkes Telescope North Photometry*

¹ Department of Physics, Broida Hall,
University of California, Santa Barbara, CA 93106, USA

² Kavli Institute for Theoretical Physics, Kohn Hall,
University of California, Santa Barbara, CA 93106, USA

³ Hubble Fellow

⁴ Las Cumbres Observatory Global Telescope Network,
6740 Cortona Drive Suite 102, Santa Barbara, CA 93117, USA

⁵ National Optical Astronomy Observatory,
950 North Cherry Avenue, Tucson, AZ 85719, USA

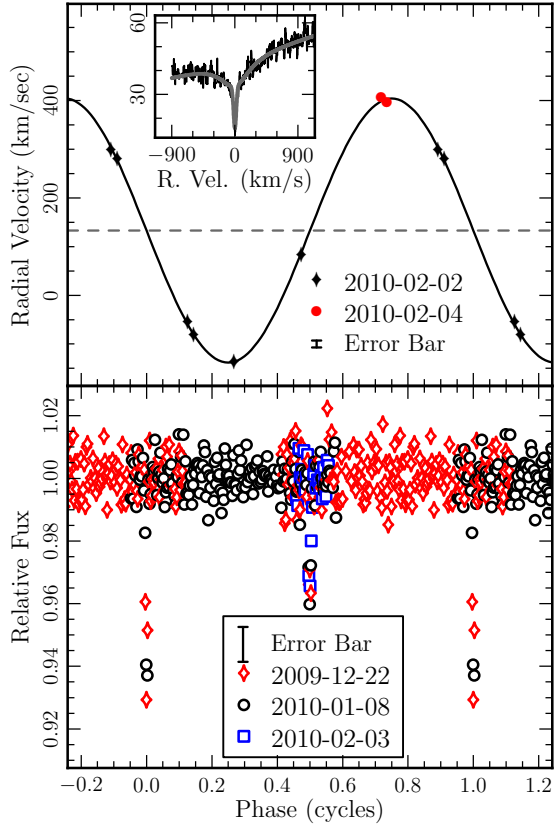


FIG. 1.— Top panel: phased radial velocities from Keck/HIRES H α measurements over two consecutive nights. The black line is the ($e = 0$) sinusoid with $K_1 = 271 \text{ km s}^{-1}$ amplitude and the $v_r = 133 \text{ km s}^{-1}$ systemic velocity offset. Inset shows the phase combined H α spectrum, in arbitrary flux units, with fitting function over plotted. Bottom panel: phased photometric light curve for all three nights of data. The error bar represents 4–5 mmag uncertainty.

Photometric observations were done with the 2 m robotic (FTN) (Lewis et al. 2010), part of the Las Cumbres Observatory Global Telescope (LCOGT) network⁶, on Haleakala, Hawaii. We used the Merope camera with 2×2 pixel binning for a pixel scale of $0''.28 \text{ pixel}^{-1}$ and a $4.75' \times 4.75'$ field-of-view. Our observational setup, consisting of the SDSS- g' filter and 45 s exposure time (with ≈ 22 s dead time), was aimed at detecting pulsations, expected to be at the few minutes timescale (Steinfadt et al. 2008b, 2010). Preliminary reduction, including bias and flat-field corrections using standard IRAF⁷ routines, is done automatically at night’s end.

Our first observation on 2009 December 22 (night 1) was for 4 hr. We immediately identified two dips in the light curve, ≈ 3 minutes in duration and a few percent in depth, indicative of eclipses. To verify the existence of eclipses we observed the system again on 2010 January 8 (night 2), for 3.5 hr, revealing two similar eclipses at the expected times based on the previous observations. An additional 30-minute observation was obtained on 2010 February 3 (night 3).

Photometric processing was carried out using IRAF aperture photometry and the VAPHOT package of routines (Deeg & Doyle 2001). Three comparison stars were selected

⁶ <http://lcogt.net>

⁷ IRAF is distributed by the National Optical Astronomy Observatory, which is operated by the Association of Universities for Research Astronomy, Inc., under cooperative agreement with the National Science Foundation. <http://iraf.noao.edu>

TABLE 1
MEASURED AND DERIVED QUANTITIES FOR NLTT 11748

Quantity	Value		
HIRES spectra			
Rad. vel. amp., K_1 (km s^{-1})	271(3)		
Sys. radial velocity, v_r (km s^{-1})	133(2)		
χ^2/dof	4.5/6		
FTN photometry			
Time of prim. ecl. (BJD TDB)	2,455,196.87828(7)		
Period (days)	0.2350606(11)		
Ephemeris χ^2/dof	3.5/3		
Primary eclipse depth, d_1	0.067(3)		
Secondary eclipse depth, d_2	0.034(2)		
Primary ecl. duration, τ_1 (s)	180(6)		
Secondary ecl. duration, τ_2 (s)	185(10)		
F_2/F_1 (in SDSS- g')	0.035(3)		
Out of eclipse ^a χ^2/dof	404.8/372		
Combined data (assuming Mass of Primary $M_1 = 0.15M_\odot$)			
Limb darkening coefficient, u_{LD}	0.0	0.3	0.5
Mass of secondary, M_2 (M_\odot)	0.71(2)	0.71(2)	0.71(2)
Inclination (deg)	89.90(11)	89.88(11)	89.87(11)
Radius of primary, R_1 (R_\odot)	0.0393(9)	0.0406(9)	0.0415(9)
χ^2/dof^b	285.1/227	279.5/227	276.5/227
Distance ^c (pc)	150(32)		
Sys. kin. (U, V, W) ^d (km s^{-1})	(-151(9), -183(41), -34(5))		

NOTE. — Quantities in parentheses are 1σ uncertainties on the last digit.

^a Excluding ± 0.005 cycles around each eclipse.

^b Result of fitting phases ± 0.1 cycles around each eclipse.

^c Scaled from Kawka & Vennes (2009) using our R_1 .

^d Calculated from the proper motion (Kawka & Vennes 2009) corrected to the local standard of rest (Hogg et al. 2005) and our updated distance.

to yield a light curve with the smallest variance. In 45 s exposures, each of these stars accumulated $\approx 4 \times 10^5 e^-$ while NLTT 11748 accumulated $\approx 7 \times 10^5 e^-$. The differential light curve for NLTT 11748 was constructed using the scheme detailed in Steinfadt et al. (2008b, inspired by Sokoloski et al. 2001). A de-trending second-order polynomial removed uncorrected long-term variations, such as color–airmass effects. For all data points outside of eclipses we find a χ^2/dof of 404.8/372, indicating a reasonable estimate of our uncertainties.

After considering the radial velocity measurements in Section 2.2, we found that nights 1 and 2 had primary and secondary eclipses, while night 3 shows a secondary eclipse. Using the technique of Kwee & van Woerden (1956) we fit the transit centers of each eclipse, and combined all eclipse timings (primary (BJD TDB): 2,455,188.886207(89), 2,455,205.81071(29); secondary (BJD TDB): 2,455,188.76882(16), 2,455,205.92783(19), 2,455,231.784879(19)) in a linear least-squares analysis to find the orbital period of $P_{\text{orb}} = 5.641454 \pm 0.000026$ hr (barycentering used the JPL DE405 ephemeris). Fitting ephemerides using the primary and secondary eclipses separately gives consistent results with our reported ephemeris (Table 1). The resulting phased light curve from all three nights of data is shown in Figure 1.

2.2. Keck Spectroscopy

We observed NLTT 11748 with High Resolution Echelle Spectrometer (HIRES, Vogt et al. 1994) on the 10-m Keck I telescope 6 times on 2010 February 2 and twice on 2010

February 4. All observations were taken with the same grating tilt, integrating for 5 minutes, binning by 3 pixels in the spatial direction, and with a $0''.86 \times 14''$ slit (giving $R \approx 50,000$). The wavelength solution was based on a Th–Ar lamp, accurate to < 0.1 pixel (with $1.4 \text{ km s}^{-1} \text{ pixel}^{-1}$), and the data covered $3600\text{--}8000 \text{ \AA}$. The stability of the solution was monitored to high precision by G. Marcy (private communication, 2010).

We used the $\text{H}\alpha$ line for our radial velocity measurements, although other lines were detected at lower significance. We initially identified the velocity from each spectrum by eye, then shifted each spectrum to zero velocity and combined them. We fit the combined $\text{H}\alpha$ spectrum with the sum of a broad ($\approx 520 \text{ km s}^{-1}$ FWHM) Lorentzian and a narrow ($\approx 47 \text{ km s}^{-1}$ FWHM) Gaussian with roughly equal depths. Using this template, we then measured radial velocities and fit them to a sinusoid with the period and phase constrained by the eclipse timing. We then iterated this procedure, using the velocities from the radial-velocity fit to construct the template, fitting the template shape, fitting the individual velocities, and fitting the radial velocity curve. This converged quickly: after one iteration all changes were $< 1 \text{ km s}^{-1}$.

We obtain a χ^2 for the radial velocity fit (assuming a circular orbit and an accurate ephemeris from the eclipse photometry) of 4.5 for 6 dof. Our final radial-velocity amplitude was $K_1 = 271 \pm 3 \text{ km s}^{-1}$ yielding a mass function $0.48(2) M_\odot$, or an $M_2 = 0.71(2) M_\odot$ secondary for a fiducial $M_1 = 0.15 M_\odot$ primary. We computed the systemic radial velocity from the data, correcting to the solar system barycenter, finding $v_r = 133 \pm 2 \text{ km s}^{-1}$. We do not correct for gravitational redshift as uncertainties in M_1 and R_1 are too high and we expect a shift of only $\approx 2 \text{ km s}^{-1}$. We checked our velocities by fitting only the broad component of the $\text{H}\alpha$ line or the $\text{H}\gamma$ line, and both gave consistent results although with a factor of 6 lower precision. We limit the eccentricity of the orbit to < 0.06 at 3σ .

At the primary’s orbital velocity, the width of the narrow $\text{H}\alpha$ component may be broadened by orbital motion: the maximum derivative is $2\pi K_1/P_{\text{orb}} = 0.08 \text{ km s}^{-1} \text{ s}^{-1}$. Compared with the narrow $\text{H}\alpha$ component, $\approx 47 \text{ km s}^{-1}$ FWHM, this effect is unlikely to affect our data (5-minute exposures) but might have slightly influenced the $\log g$ measurement of Kawka & Vennes (2009).

3. BINARY PARAMETER ANALYSIS AND RESULTS

The deepest (primary) eclipse is the transit of the primary object (1) by the secondary (2), and the shallowest (secondary) is the occultation of the secondary by the primary. There are six relevant binary parameters to be fitted: the primary and secondary radii and masses (R_1 , R_2 , M_1 and M_2); flux ratio (for our filter/CCD response) F_2/F_1 ; and inclination i . We consider the orbital period, P_{orb} , and the linear limb darkening coefficient, u_{LD} , as fixed. We presume $u_{\text{LD}} = 0.3$ but will show how its uncertainty ($u_{\text{LD}} \approx 0.2\text{--}0.6$, Littlefair et al. 2006, 2007, and Maxted et al. 2007) modifies our desired parameters. The eclipse light curve in Figure 2 shows the secondary eclipse as flat-bottomed while the primary eclipse shows the distinct signature of limb darkening. This indicates that the eclipses are likely total (confirmed by our inclination measurements) and $R_2 < R_1$, $F_2/F_1 \ll 1$, and $i \approx 90^\circ$.

We initially fit the eclipses with a parameterization of the linear limb darkening law (Van Hamme 1993) for the primary eclipse and a box function for the total secondary eclipse,

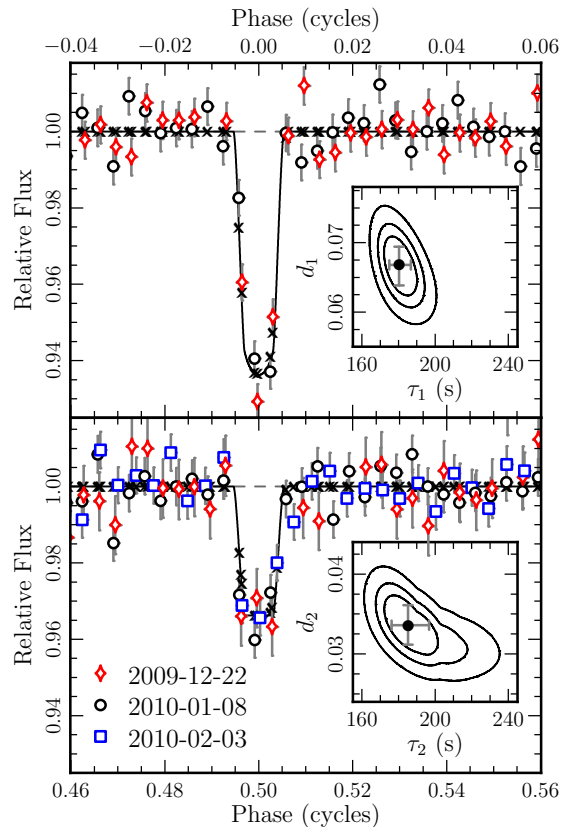


FIG. 2.— Phased light curves of the primary (top panel) and secondary (bottom panel) eclipses. The widths of each data point represent the exposure duration. The black line is the light curve model for the $u_{\text{LD}} = 0.3$ parameters in Table 1. The crosses show the average of the model over the exposure duration of that associated data point. It is the differences between these points and those measurements that are considered when calculating χ^2 . Insets display the 1σ , 2σ , and 3σ contours of the χ^2 minimization for the eclipse depth and width parameterized light curve fitting. The error bars are the 1σ error bars on the individual parameters.

yielding the depths, d_1 and d_2 , and durations, τ_1 and τ_2 . The 1σ results are reported in Table 1 with the 1σ , 2σ , and 3σ contours plotted in the insets of Figure 2. This allows us to directly measure F_2/F_1 , as $1 - d_2 = F_1/(F_1 + F_2)$.

The sparsity of our data in eclipse requires additional assumptions about the properties of the secondary. The flat bottom secondary eclipse unambiguously gives a low flux ratio (at SDSS- g') of $F_2/F_1 = 0.035(3)$ which implies that the value of the primary eclipse total depth must be dominated by the radii ratio. Our measured primary eclipse depth implies $R_2/R_1 \approx 1/4$, further corroborated by the unseen (and thereby fast) ingress and egress in the secondary eclipse. Our measurements of F_2/F_1 and R_2/R_1 constrain the temperature of the secondary relative to the 8500 K primary. Taking SDSS- g' measurements as bolometric ($L_2/L_1 = F_2/F_1$) gives $T_2 \leq 7400 \text{ K}$, which we confirm by using the synthetic photometry of Holberg & Bergeron (2006), constraining the flux ratio of model atmospheres integrated over the filter passband. The Kawka & Vennes (2009) spectrum constrains the primary to be a low-mass, $\lesssim 0.25 M_\odot$, likely He WD with a radius $\approx 0.04 R_\odot$. This implies an $R_2 \approx 0.01 R_\odot$ companion. Therefore, the secondary cannot be a main sequence (MS) star as Kawka & Vennes (2009) constrain such an MS star to have $M < 0.2 M_\odot$ based on Two Micron All Sky Survey photometry, breaking our mass function and radius constraints. A

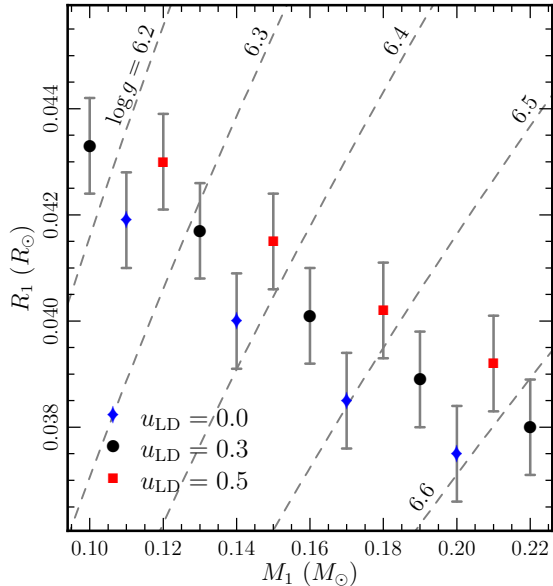


FIG. 3.— Primary radius vs. primary mass. The uncertainties are 1σ uncertainties assuming the values and uncertainties of K_1 and F_2/F_1 given in Table 1 and assuming a secondary radius derived from its mass. Dashed lines are constant $\log g$.

brown dwarf would break our mass function and radius constraints. A neutron star is far too small and its luminosity contribution insufficient. Therefore, a cold C/O WD is the only solution, meeting the radius, mass, and luminosity constraints.

We powerfully constrain the binary parameters by directly integrating the faces of the primary and secondary and model our light curve for any arbitrary inclination and phase by assuming a linear limb darkening law. We do this with a code originating from Steinfadt et al. (2008a) and Mandel & Agol (2002), including the effects of microlensing in the binary (following Marsh 2001 and Agol 2002). For the approximate parameters above, the Einstein radius is $R_E = \sqrt{4GM_2a/c^2} \approx 0.003 R_\odot$, giving $R_1/R_E \approx 13$ and $R_2/R_E \approx 3$, leading to a 1% magnification of the primary at conjunction. Our measurement of K_1 and F_2/F_1 reduces our six-parameter system to four-parameter system. Our surface temperature measurement yields an age of 1.5–3.0 Gyr (Chabrier et al. 2000) for the secondary allowing us to use M-R relations of cold WDs (Althaus & Benvenuto 1998) for our current work. Though Kawka & Vennes (2009) derived an $M_1 = 0.167 \pm 0.005 M_\odot$ from their low-resolution spectrum, radial velocity broadening and theoretical model uncertainties may render this determination unreliable. Therefore, we calculate separate χ^2 grids of R_1 and inclination for a range of M_1 . Minimization of χ^2 on each grid constrains R_1 and inclination directly and $\Delta\chi^2$ techniques yield their uncertainties. We scale these uncertainties to consider the additional uncertainties of F_2/F_1 and K_1 using a Monte Carlo method.

The results of our direct eclipse fitting method are displayed in Figure 3 with the parameters and uncertainties reported in Table 1 for $M_1 = 0.15 M_\odot$. Without including lensing the fits would be very similar, but the inclination would be slightly lower (closer to 89.4°) and the radius of the primary would be slightly larger ($0.0437 R_\odot$ for $u_{LD} = 0.3$). The χ^2 minima for all M_1 within each u_{LD} data set in Figure 3 are approximately consistent and as such yield no constraint on M_1

over this range. Our range of $u_{LD} = 0.0, 0.3, \text{ and } 0.5$ results in a $\approx 5\%$ spread in R_1 measurements, consistent with the $\log g = 6.2 \pm 0.15$ of Kawka & Vennes (2009). The χ^2 value is reduced slightly as u_{LD} increases; however, we cannot constrain u_{LD} due to the sparsity of data at ingress/egress. This will be constrained in future higher cadence data sets. For $M_1 > 0.2 M_\odot$ the minimum χ^2 values significantly increase and the quality of the eclipse fits degrade. Therefore, our combined radial velocity and light curve data sets provide an upper limit, assuming that the secondary is a C/O WD, of $M_1 \lesssim 0.2 M_\odot$.

4. CONCLUSIONS

Our discovery of the first eclipsing detached double WD binary has substantially constrained low-mass He WD models with radius measurements that agree with current models (Serenelli et al. 2002; Panei et al. 2007). Additional measurements will reveal even more about the faint $\approx 0.7 M_\odot$ C/O WD secondary. With our discovery, there are 11 confirmed double WD binaries that will merge within a Hubble time. From spectroscopic masses alone, six of these contain low-mass ($< 0.25 M_\odot$) He core primaries with large ($> 0.03 R_\odot$) radii indicative of a stable H burning shell (Mullally et al. 2009; Kilic et al. 2009; Badenes et al. 2009; Marsh et al. 2010; Kulkarni & van Kerkwijk 2010). Other than its inclination, NLTT 11748 is not extraordinary in any way relative to these, many of which offer larger solid angles for eclipse observations than NLTT 11748.

Our analysis of this system is far from complete, but our existing constraints, Table 1 and Figure 3, highlight the value of further studies. High cadence photometry, resolving the ingress/egress of each eclipse, would yield the component radii as functions of inclination and orbital semimajor axis. If future spectroscopic observations can reveal the secondary’s line features and measure its radial velocity, this would allow precise measurements of the masses of both components. Detection of eclipses in different filters, both bluer and into the infrared, would additionally constrain the temperature of the secondary further as well as its age.

Model-independent mass and radius determinations for He and C/O WDs are rare. For He WDs, there exist several pulsar binary systems for which Shapiro time delay measurements have yielded accurate mass determinations: PSR B1855+09 (Kaspi et al. 1994), PSR J0437–4715 (van Straten et al. 2001), PSR J0751+1807 (Bassa et al. 2006b), PSR J1012+5307 (Callanan et al. 1998; van Kerkwijk et al. 1996), PSR J1911–5958A (Bassa et al. 2006a), and PSR J1909–3744 (Jacoby et al. 2003, 2005). Of these, only four have radii measurements, PSR J0437–4715, PSR J0751+1807, PSR J1911–5958A and PSR J1909–3744. However, all rely upon either distance measurements and evolutionary model-dependent luminosities or gravity measurements derived from atmospheric models. Therefore, He WD evolutionary models (Althaus & Benvenuto 1998; Serenelli et al. 2002; Panei et al. 2007) remain largely unconstrained. For C/O WDs, mass and radius measurements have been more frequent (Schmidt 1996; Provencal et al. 1998, 2002; Casewell et al. 2009) and all rely on distance measurements via parallax or cluster membership, surface brightness measurements and detailed knowledge of each spectrum. To reach the precisions required to constrain theoretical models, these measurements must rely upon atmospheric model spectra. Only recently Parsons et al.

(2010) have derived precise measurements of mass and radius in a model-independent way in the eclipsing binary system NN Ser. NLTT 11748 offers an additional C/O WD system for model-independent mass and radius measurements as well as the first such system for He WDs.

Gravitational wave emission will bring this system into contact in $13.8-6.3$ Gyr (for $M_1 = 0.1-0.2M_\odot$). With a mass ratio of $0.15/0.71 = 0.2$, stable mass transfer at contact is likely to occur and create an AM CVn binary (Nelemans et al. 2001; Marsh et al. 2004). The known orbital period, inclination, and distance ($d \approx 150$ pc) yield the gravitational wave strain at Earth, $h = (3.6-7.9) \times 10^{-23}$ (Timpano et al. 2006; Roelofs et al. 2007) at a frequency $\nu \approx 10^{-4}$ Hz for $M_1 = 0.1-0.2M_\odot$. Though not 'louder' than the verification sources tabulated by Nelemans (2009), NLTT 11748's accurate ephemeris allows for a coherent folding of the *LISA* data over the mission duration.

We thank the referee for helpful comments and suggestions.

REFERENCES

- Agol, E. 2002, *ApJ*, 579, 430
 Althaus, L. G. & Benvenuto, O. G. 1998, *MNRAS*, 296, 206
 Badenes, C., Mullally, F., Thompson, S. E., & Lupton, R. H. 2009, *ApJ*, 707, 971
 Bassa, C. G., van Kerkwijk, M. H., Koester, D., & Verbunt, F. 2006a, *A&A*, 456, 295
 Bassa, C. G., van Kerkwijk, M. H., & Kulkarni, S. R. 2006b, *A&A*, 450, 295
 Deeg, H. J. & Doyle, L. R. 2001, in *Third Workshop on Photometry*, ed. W. Borucki & L. E. Lasher, Ames Research Center: NASA NASA/CP-2000-209614, 85
 Driebe, T., Blöcker, T., Schönberner, D., & Herwig, F. 1999, *A&A*, 350, 89
 Callanan, P. J., Garnavich, P. M., & Koester, D. 1998, *MNRAS*, 298, 207
 Casewell, S. L., Dobbie, P. D., Napiwotzki, R., Burleigh, M. R., Barstow, M. A., & Jameson, R. F. 2009, *MNRAS*, 395, 1795
 Chabrier, G., Brassard, P., Fontaine, G., & Saumon, D. 2000, *ApJ*, 543, 216
 Hogg, D. W., Blanton, M. R., Roweis, S. T., & Johnston, K. V. 2005, *ApJ*, 629, 268
 Holberg, J. B., & Bergeron, P. 2006, *AJ*, 132, 1221
 Iben, I., Jr., & Tutukov, A. V. 1984, *ApJS*, 54, 335
 Jacoby, B. A., Bailes, M., van Kerkwijk, M. H., Ord, S., Hotan, A., Kulkarni, S. R., & Anderson, S. B. 2003, *ApJ*, 599, L99
 Jacoby, B. A., Hotan, A., Bailes, M., Ord, S., & Kulkarni, S. R. 2005, *ApJ*, 629, L113
 Kaspi, V. M., Taylor, J. H., & Ryba, M. F. 1994, *ApJ*, 428, 713
 Kawka, A., & Vennes, S. 2009, *A&A*, 506, L25
 Kawka, A., Vennes, S., Oswalt, T. D., Smith, J. A., & Silvestri, N. M. 2006, *ApJ*, 643, L123
 Kilic, M., Allende Prieto, C., Brown, W. R., & Koester, D. 2007, *ApJ*, 660, 1451
 Kilic, M., Brown, W. R., Allende Prieto, C., Kenyon, S. J., & Panei, J. A. 2009, arXiv:0911.1781
 Kulkarni, S. R., & van Kerkwijk, M. H. 2010, arXiv:1003.2169
 Kwee, K. K. & van Woerden, H. 1956, *Bull. Astron. Inst. Netherlands*, 464, 327
 Lewis, F., Street, R., Roche, P., Stroud, V., & Russell, D. M. 2010, *Advances in Astronomy*, 2010, 1
 Littlefair, S. P., Dhillon, V. S., Marsh, T. R., Gänsicke, B. T. 2006, *MNRAS*, 371, 1435
 Littlefair, S. P., Dhillon, V. S., Marsh, T. R., Gänsicke, B. T., Baraffe, I., & Watson, C. A. 2007, *MNRAS*, 381, 827
- Mandel, K., & Agol, E. 2002, *ApJ*, 580, L171
 Marsh, T. R. 2001, *MNRAS*, 324, 547
 Marsh, T. R., Gaensicke, B. T., Steeghs, D., Southworth, J., Koester, D., Harris, V., & Merry, L. 2010, arXiv:1002.4677
 Marsh, T. R., Nelemans, G., & Steeghs, D. 2004, *MNRAS*, 350, 113
 Maxted, P. F. L., O'Donoghue, D., Morales-Rueda, L., Napiwotzki, R., & Smalley, B. 2007, *MNRAS*, 376, 919
 Mullally, F., Badenes, C., Thompson, S. E., & Lupton, R. 2009, *ApJ*, 707, L51
 Nelemans, G. 2009, *Class. and Quantum Grav.*, 26, 094030
 Nelemans, G., Yungelson, L. R., Portegies Zwart, S. F., & Verbunt, F. 2001, *A&A*, 365, 491
 Panei, J. A., Althaus, L. G., Chen, X., & Han, Z. 2007, *MNRAS*, 382, 779
 Parsons, S. G., Marsh, T. R., Copperwheat, C. M., Dhillon, V. S., Littlefair, S. P., Gänsicke, B. T., & Hickman, R. 2010, *MNRAS*, 402, 2591
 Provencal, J. L., Shipman, H. L., Hog, E., & Thejll, P. 1998, *ApJ*, 494, 759
 Provencal, J. L., Shipman, H. L., Koester, D., Wesemael, F., & Bergeron, P. 2002, *ApJ*, 568, 324
 Roelofs, G. H. A., Groot, P. J., Benedict, G. F., McArthur, B. E., Steeghs, D., Morales-Rueda, L., Marsh, T. R., & Nelemans, G. 2007, *ApJ*, 666, 1174
 Schmidt, H. 1996, *A&A*, 311, 852
 Serenelli, A. M., Althaus, L. G., Rohrmann, R. D., & Benvenuto, O. G. 2002, *MNRAS*, 337, 1091
 Sokoloski, J. L., Bildsten, L., & Ho, W. C. G. 2001, *MNRAS*, 326, 553
 Steinfadt, J. D. R., Bildsten, L., & Howell, S. B. 2008a, *ApJ*, 677, L113
 Steinfadt, J. D. R., Bildsten, L., Ofek, E. O., & Kulkarni, S. R. 2008b, *PASP*, 120, 1103
 Steinfadt, J. D. R., Bildsten, L., & Arras, P. 2010. In preparation.
 Timpano, S. E., Rubbo, L. J., & Cornish, N. J. 2006, *Phys. Rev. D.*, 73, 122001
 Van Hamme, W. 1993, *AJ*, 106, 2096
 van Kerkwijk, M. H., Bergeron, P., & Kulkarni, S. R. 1996, *ApJ*, 467, L89
 van Straten, W., Bailes, M., Britton, M., Kulkarni, S. R., Anderson, S. B., Manchester, R. N., & Sarkissian, J. 2001, *Nature*, 412, 158
 Vogt, S. S., et al. 1994, *Proc. SPIE*, 2198, 362
 Webbink, R. F. 1984, *ApJ*, 277, 355